Engineering 19 (2022) 84–92

Contents lists available at ScienceDirect

Engineering

journal homepage: www.elsevier.com/locate/eng

Research
Material Engineering—Article

Transformation of Fibrous Membranes from Opaque to Transparent under Mechanical Pressing

Chao Wang [a], Jing Zhao [a], Liu Liu [b], Peng Zhang [c], Xianfeng Wang [a,b,*], Jianyong Yu [b], Bin Ding [a,b,*]

[a] State Key Laboratory for Modification of Chemical Fibers and Polymer Materials, College of Textiles, Donghua University, Shanghai 201620, China
[b] Innovation Center for Textile Science and Technology, Donghua University, Shanghai 200051, China
[c] State Center for International Cooperation on Designer Low-carbon and Environmental Materials, School of Materials Science and Engineering, Zhengzhou University, Zhengzhou 450001, China

ARTICLE INFO

Article history:
Received 31 July 2020
Revised 8 January 2021
Accepted 6 February 2021
Available online 21 May 2021

Keywords:
Transparent
Electrospun fibrous membranes
Porous structure
Mechanical pressing
Conductivity

ABSTRACT

There is a great demand for transparent films, membranes, or substrates in the fields of intelligent wearables, electronic skins, air filtration, and tissue engineering. Traditional materials such as glass and plastics cannot satisfy these requirements because of the lack of interconnected pores, undesirable porosity, and flexibility. Electrospun fibrous membranes offset these shortcomings because they contain small pores and have high porosity as well as outstanding flexibility. Thus, the development of transparent electrospun fibrous membranes is of great value. This work reports a simple and effective way to develop flexible and porous transparent fibrous membranes (TFMs) directly from electrospun fibrous membranes via mechanical pressing, without employing any other additives. In addition, the relationship between the transparency performance and the molecular structure of the polymers after pressing was summarized for the first time. After mechanical pressing, the membranes maintained fibrous morphology, micron-sized pores, and desired porosity. Polystyrene fibrous membranes, which exhibited excellent optical and mechanical properties, were used as a reference. The TFMs possessed high transparency (~89% visible light transmittance at 550 nm), high porosity (10%–30%), and strong mechanical tensile strength (~148 MPa), nearly 78 times that of the pristine electrospun fibrous membranes. Moreover, this study demonstrated that transparent and conductive membranes can be fabricated based on TFMs using vacuum-assisted filtration of silver nanowires followed by mechanical pressing. Compared with indium tin oxide films, conductive TFMs exhibited good electrical conductivities (9 Ω per square ($\Omega \cdot sq^{-1}$), 78% transmittance at 550 nm) and notable mechanical performance (to bear abundant bending stresses).

1. Introduction

Flexible, transparent films, membranes, and substrates have attracted extensive attention in a variety of fields, including smart wearables, electronic skins, and air filtration [1–4]. Traditional transparent films or substrates, such as glass, polyester (PET), or polyethylene plastic, cannot completely meet the demands of emerging application areas that require interconnected pores, high porosity, and flexibility. For example, as smart wearables or electronic skins gain popularity, the currently available transparent films cannot fulfill the demands because they cannot simultaneously exhibit high transmittance and excellent breathability [5–7]. In other applications involving human health being vulnerable to particulate matter pollution, existing filter materials such as window gauze have a high filtration performance but poor light transmittance [8,9]. In addition, the emergence of coronavirus disease 2019 (COVID-19) has proved the vital importance of face masks with high sterilization and filtration performance, but their low light transmittance interferes with communication between healthcare workers and people. Therefore, it is worth developing transparent face masks to fight COVID-19 [10]. Recently, new types of transparent materials have attracted significant attention. In particular, transparent and flexible cellulose nanopaper [11–15] and chitin [16,17] nanofibers have been developed. The nanopaper exhibited high optical transmittance and good mechanical performance and was expected to replace traditional plastic films.

* Corresponding authors.
E-mail addresses: wxf@dhu.edu.cn (X. Wang), binding@dhu.edu.cn (B. Ding).

https://doi.org/10.1016/j.eng.2021.02.018

However, the manufacturing process for the nanopaper involves a complicated chemical treatment, and the resulting material has an inadequate porous structure or no pores. Wood is also a versatile material that has been used in many applications, and transparent wood films have even been reported [18–23] to have exceptional performance, better than traditional glass. Nevertheless, these films also lack interconnected pores and require complex chemical processing, which consumes energy and time. Consequently, transparent materials with a porous structure fabricated via a low-cost and simple approach are difficult to obtain but are urgently needed.

The electrospinning technique allows for the easily scalable synthesis of continuous micro- or nanofibers from diverse materials such as polymers [24–26], carbon [27–29], and ceramics [30–32], and has been confirmed to be an effective method for manufacturing micro- or nanofibers [33–35]. The resulting electrospun membranes possess small pores, high porosity, excellent flexibility, and robust mechanical properties [34]. Therefore, the fabrication of transparent electrospun fibrous membranes is a promising approach for achieving the above functions. However, it is extremely difficult to obtain transparent electrospun membranes owing to light reflection and scattering from the micro- and nanofibers.

Studies of transparent electrospun fibrous membranes have been reported, and the fabrication methods of these functional materials can be divided into two categories. One method involves filling a polymer into fibrous membranes, which can generate transparent nanocomposites. For example, a two-component phenolic epoxy resin was incorporated into an electrospun nylon-4,6 membrane [36], a nylon-6 nanofibrous membrane was filled with cellulose acetate (CA) [37], and a polyacrylonitrile (PAN)/polyurethane (PU) composite nanofibrous membrane was heated to melt the PU and achieve transparency [38]. This method for transparent fibrous membrane (TFM) fabrication results in loss of fibrous structures and pores, while the micro- or nanofibers act as the only reinforcement. The other methodology involves decreasing the thickness of the electrospun fibrous membranes. The thinner the fibrous membrane, the higher the light transmittance. One example is the fabrication of an ultrathin nanofiber or nanonet membrane air filter with high performance by combining the electrospinning/netting technique [39–45]. However, the shortcomings include poor mechanical properties and harsh process conditions, hence the fabrication process is time-consuming and the nanonet membranes cannot be used independently. Therefore, the existing methods of fabricating electrospun TFMs are complex and lose the advantages of fibrous membranes. Thus, the development of pure and free-standing transparent electrospun membranes remains a challenge.

In this study, a facile and effective strategy for creating electrospun TFMs via mechanical pressing was demonstrated, and the relationship between transparency and polymer chain structures was summarized for the first time. After pressing, the TFMs maintained their fibrous morphology, had micron-sized pores, and possessed the desired porosity. In addition, the porosity, pore size, and light transmittance of the membranes could be regulated using pressure. The obtained TFMs exhibited excellent flexibility, optical transmittance, and mechanical properties. However, the limitation of this method is that the fibers are easily damaged, which should be addressed in future work. Transparent nanocomposite conductive membranes based on TFMs utilizing vacuum-assisted filtration of silver nanowires (AgNWs) were also realized. The resulting transparent conductive electrodes showed high electrical conductivity and notable mechanical performance.

2. Materials and methods

2.1. Materials

Polysulfone (PSU; molecular weight (M_w) = 67 000) polymer chips, polystyrene (PS; M_w = 350 000) polymer chips, polyvinylidene fluoride (PVDF; M_w = 1 050 000), CA (M_w = 30 000), dimethylformamide (DMF, analytical reagent (AR)), acetone, dimethyl sulfoxide (DMSO), and ethanol (EtOH, 99%) were purchased from Aladdin Chemistry Co., Ltd., China. PAN (M_w = 90 000) was purchased from Kaneka Co., Ltd., Japan. PU (IROGRAN A 85 P 4394 FCM) was purchased from Huntsman Co., Ltd., Germany. AgNW (10 $mg{\cdot}mL^{-1}$) solution was purchased from Shanghai Puwei Applied Materials Technology Co., Ltd., China. These chemicals were used directly without further purification. Indium tin oxide (ITO) films (150 Ω per square ($\Omega{\cdot}sq^{-1}$)) were obtained from Shanghai Keyan Phosphor Technology Co., Ltd., China.

2.2. Preparation of polystyrene (PS) TFMs

First, PS polymer chips (8.4 g) were dissolved in DMF (31.6 g) with stirring for 8 h to prepare the PS electrospinning solution. Then, the solution was transferred to a plastic syringe, which was subsequently fixed onto a DXES-4 electrospinner (Shanghai Oriental Nanotechnology Co., Ltd., China) equipped with a high-voltage power supply. A piece of nonwoven fabric was covered with a metallic cylinder as the collector. The feeding rate was 3 $mL{\cdot}h^{-1}$, the voltage applied to the spinneret was 30 kV, the distance between the spinneret and the collector was 20 cm, and the rotation rate of the cylinder was 50 revolutions per minute (rpm). The temperature and relative humidity were controlled at (23 ± 2) °C and 80% ± 3%, respectively. Therefore, fluffy PS fibrous membranes were formed. Then, different pressures in the range of 0–35 MPa were applied to the membranes for 10 min to obtain PS TFMs with different transparencies.

2.3. Fabrication of PS TFM/AgNWs conductive films

The silver nanowire dispersions were prepared first. AgNWs with the average diameter of 30 nm and length of 100 μm were chosen and dispersed in ethanol at the concentration of 0.2 $mg{\cdot}mL^{-1}$ and then subjected to ultrasonication for 15 s. Then, the fluffy PS fibrous membrane was cut into small pieces with a diameter (d) of 20 mm. Afterward, the samples were hot-pressed at 0.5 MPa and 40 °C for 5 s to obtain a dense and smooth surface. Then, different amounts of AgNWs were loaded onto the surface via vacuum filtration followed by oven drying at 40 °C for 1 h. Finally, PS samples with AgNWs were pressed using different pressures to obtain PS TFM/AgNW conductive films.

2.4. Characterizations

Scanning electron microscopy (SEM) images were obtained using a VEGA 3 SEM instrument (TESCAN Ltd., Czech Republic). The root-mean-square (RMS) roughness of the films and single fibers of the TFM were tested using optical profilometry (Bruker ContourGT-K1, Germany) and atomic force microscopy (AFM, Agilent 5500, USA). The pore structures of the membranes were investigated using a capillary flow porometer (CFP-1100AI, Porous Materials Inc., Germany). The porosities of the obtained films were computed using the following formula:

$$\text{Porosity} = \frac{\rho_1 - \rho_2}{\rho_1} \times 100\% \quad (1)$$

where ρ_1 and ρ_2 represent the densities of the polymer and the electrospun membranes, respectively. The tensile mechanical properties of the membranes were analyzed using a tensile tester (XQ-1C, Shanghai New Fiber Instrument Co., Ltd., China). X-ray diffractometry (XRD) measurements were performed on a D8 Advance diffractometer (Bruker, Germany), using CuKα (wavelength of 1.5406 Å (1 Å = 10^{-10} m)) as the X-ray source. The transmittance spectra were measured using a ultraviolet–visible (UV–vis) spectrometer (U-3900, Hitachi, Japan). Furthermore, the sheet resistance was measured using a multifunction digital four-probe tester (ST-2258C, Suzhou Jingge Electronic Co., Ltd., China).

3. Results and discussion

The TFM fabrication process includes two steps, which are simple and consume little energy and time, as shown in Fig. 1(a). In the first step, one polymer was selected as the primary material to prepare a continuous fibrous network via electrospinning. After a few hours, the pristine fibrous membrane was fabricated under suitable spinning conditions. In the second step, mechanical pressing was applied to the free-standing fluffy fibrous network for a few minutes. This led to a reduction in thickness, and thus, a highly TFMs. Using this facile method, various fibrous polymers and

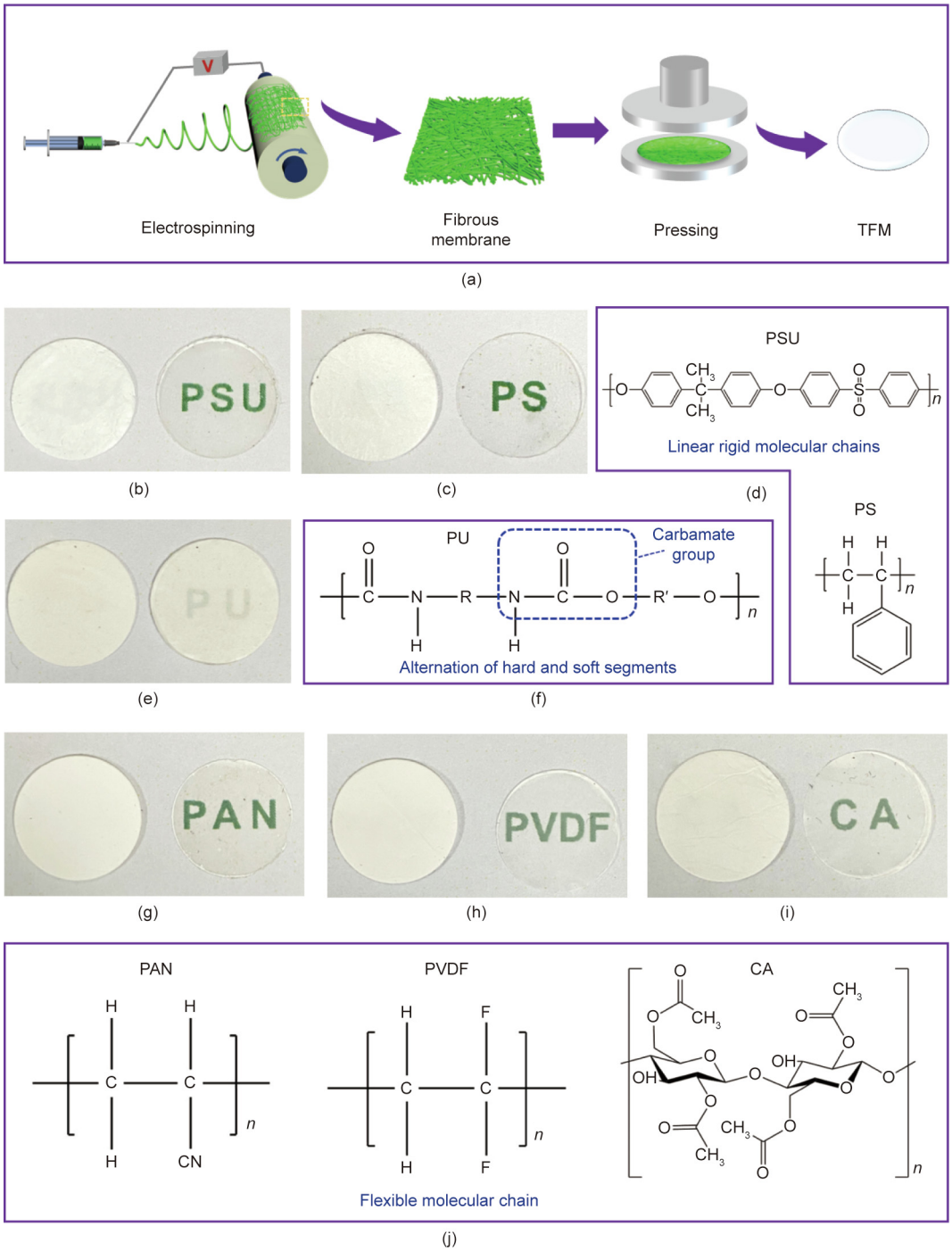

Fig. 1. Fabrication process of TFMs. (a) Schematic of TFM fabrication. Photographs of (b) PSU and (c) PS fibrous membranes before and after pressing (d = 20 mm). (d) Molecular structures of PSU and PS. (e) Photographs of PU fibrous membranes before and after pressing (d = 20 mm). (f) Molecular structure of PU. Photographs of (g) PAN, (h) PVDF, and (i) CA fibrous membranes before and after pressing (d = 20 mm). (j) Molecular structures of PAN, PVDF, and CA.

free-standing TFMs could be fabricated, and the light transmittance was controlled by pressing at different mechanical pressures. According to the relationship between the transparency and flexibility of molecular chains, the polymers frequently used in electrospinning can generally be divided into three categories (Figs. 1(b)–(j)). In the first category, linear polymers with rigid molecular chains that contain benzene rings in the backbone or side chains exhibit the best transparent performance for fibrous membranes after pressing. This is because the polymer chains feature a high rigidity (internal rotation of chemical bonds is not allowed) and are more prone to brittle deformation under external force, leading to densely packed fibrous membranes. For example, as shown in Figs. 1(b) and (c), the PSU and PS fibrous membranes with rigid polymer chains (Fig. 1(d)) reached the highest transparency after pressing. In the second category, the block copolymer PU is composed of alternately inlaid soft and hard segments, so it displays polymer chains with flexibility and resilience (chemical bonds are easier to rotate and recover). As a result, the fibers were more difficult to deform, and therefore, the fibrous membranes had very poor transparency after pressing (Fig. 1(e)). As shown in Fig. 1(f), the repeat unit of PU is the carbamate group (–NHCOO–), whose left and right ends are hard and soft segments, respectively. In the third category, polymers with fine molecular chains exhibited flexibility between the other two types of polymers and exhibited high membrane transparency after pressing. For example, as shown in Figs. 1(g)–(i), PAN, PVDF, and CA fibrous membranes also exhibited high transparency after pressing, better than the block copolymer PU but lower than the linear, rigid polymers (PSU and PS). The molecular structures of the polymers are shown in Fig. 1(j). The average thickness of all the fibrous membranes was controlled at approximately (80 ± 2) μm.

It should be emphasized that this classification applies to most polymers used in electrospinning, except for a few special cases, and the thicknesses and average fiber diameters of the above pristine membranes were controlled at the same scale (Figs. S1 and S2 in Appendix A). In addition, pressed TFMs are mechanically flexible and can easily attach to different substrates. Appendix A Fig. S3 shows examples of TFMs that were successfully transferred to various surfaces, such as a leaf, paper napkin, PET plastic, and curved glass. These transfers were all performed without any surface treatment, indicating that the transparent membranes have favorable adhesion properties.

Here, PS fibrous membranes were used as an example to study the performance of TFMs. Figs. 2(a)–(d) shows the SEM images of the pristine PS membrane and three types of pure PS TFMs with different light transmittances (at 550 nm). The light transmittance of the untreated pristine PS membrane was approximately 0.1%, indicating that the light could barely pass through the membrane. Corresponding to the different mechanical pressures of 25, 30, and 35 MPa, the light transmittances of the three TFMs were 78%, 83%, and 89%, respectively at 550 nm. From the optical photos, we can see a significant difference in transparency (Appendix A Fig. S4). Fig. 2(a) indicates that the pristine PS membrane had a sparse and loose fibrous structure with a large size and large number of pores. Figs. 2(b)–(d) show that the TFMs were compact, and the size and number of pores were considerably decreased.

However, with the increase in light transmittance, the loss of fibrous morphology also increases, as shown in Figs. 2(b)–(d). This is because the fibers are flattened and partially embedded in each other (Appendix A Fig. S5). The pore size distribution and porosity of the membranes were also studied, and the results are presented in Fig. 2(e). The pore size distribution of the pristine PS membrane was in the range of 10–20 μm, while the porosity and transmittance were 98.1% and 0.1%, respectively. After pressing, the pore size was reduced to the range of 0.4–2.0 μm, while the membrane possessed 27.7% porosity and 78.0% transmittance. As the transmittance increased, the pore size became smaller and more concentrated to the range of 0.2–1.5 μm, and a decrease in the porosity was observed to 23.2% with 83.0% transmittance. When the porosity decreased to 10.2%, the transmittance was 89.0% and the pore size was 0.1–0.9 μm. Hence, the pore size and porosity decrease with an increase in the light transmittance. The porosity changed significantly from 98.1% to 10.2%, while the light transmittance increased from 0.1% to 89.0%. The relationship between porosity and transmittance is shown in Fig. 2(f). The corresponding porosity values of the different transmittances are listed in Appendix A Table S1, which proves that porosity is the main contributor to transparency. Appendix A Fig. S6 shows the transmittance and thickness of the PS TFMs fabricated at different pressures. When the pressure was increased from 0 to 35 MPa, the transmittance increased from 0.1% to 89.0%, and the thickness decreased from approximately 1300 to 23 μm. As the pressure continued to increase, the light transmittance hardly changed, but the fibrous membranes were destroyed. As shown in Fig. 2(g), AFM was used to collect the surface information of a single fiber from the 89.0%-transmittance membrane, and it was found that the single fiber had a low RMS of (52 ± 2) nm. A three-dimensional (3D) AFM line scan image of the PS TFM is displayed in Appendix A Fig. S7. Moreover, as shown in Figs. 2(h)–(k), 3D optical profilometry images of Figs. 2(a)–(d) were obtained, while the 2D optical profilometry images are shown in Appendix A Fig. S8. It can be seen that the pristine membrane had a high surface roughness with the RMS of (8.98 ± 1.00) μm. The pristine membrane comprised many PS micro/nanofibers with countless micro-sized pores, which led to intense light reflection and scattering loss at numerous fiber–air interfaces. Therefore, the pristine membrane displayed high opacity. Compared with the pristine membrane, the transparent membranes became denser with low surface roughness and smaller pores after pressing. The RMS values of the membranes with transmittances of 78.0%, 83.0%, and 89.0% were (319 ± 10), (278 ± 10), and (176 ± 10) nm, respectively. This indicates that the transparency increased while the surface roughness decreased.

Therefore, within a proper range, the greater the applied pressure, the higher the light transmittance achieved by the membrane. Although high pressure caused closer packing of fibers and reduced surface roughness, thickness, and pore size, as well as decreased fibrous morphology to a certain degree, the TFMs maintained a certain porosity and fibrous morphology and did not form solid films. This phenomenon has also been observed in TFMs made from other polymers. Compared with traditional solid and smooth transparent films, such as PET board and glass, porous TFMs possess the advantages of high porosity, controllable pore sizes, and prospective applications in the fields of flexible electronics, tissue engineering, and air filtration, among others.

According to the research and analysis presented above, the reasons why the fibrous membrane materials are opaque will be explained here, as well as the mechanism for the development of transparency in the fibrous membrane materials (Fig. 3(a)). When light passes through the fibrous membrane, there are several losses: absorption loss (some light is absorbed by the fibrous membrane), reflection loss (light is reflected back onto the surface of the fibrous membrane), scattering loss (inside the fibrous membrane), and the direct transmittance of light. The main factors that affected the light transmittance of the fibrous membranes were as follows: ① surface roughness of the fibrous membrane. Defects (cracks and pores) and dust particles on the surfaces of the fibers increased the roughness of the entire membrane, which caused the light to diffuse and reflect off the surface. In addition, the structure of the accumulated fibers affected the surface roughness. The denser and smoother the accumulated fibers, the lower the surface roughness of the fibrous membrane. ② Air. The fibrous membrane is a mixture of fibers and air. The different refractive indices of air

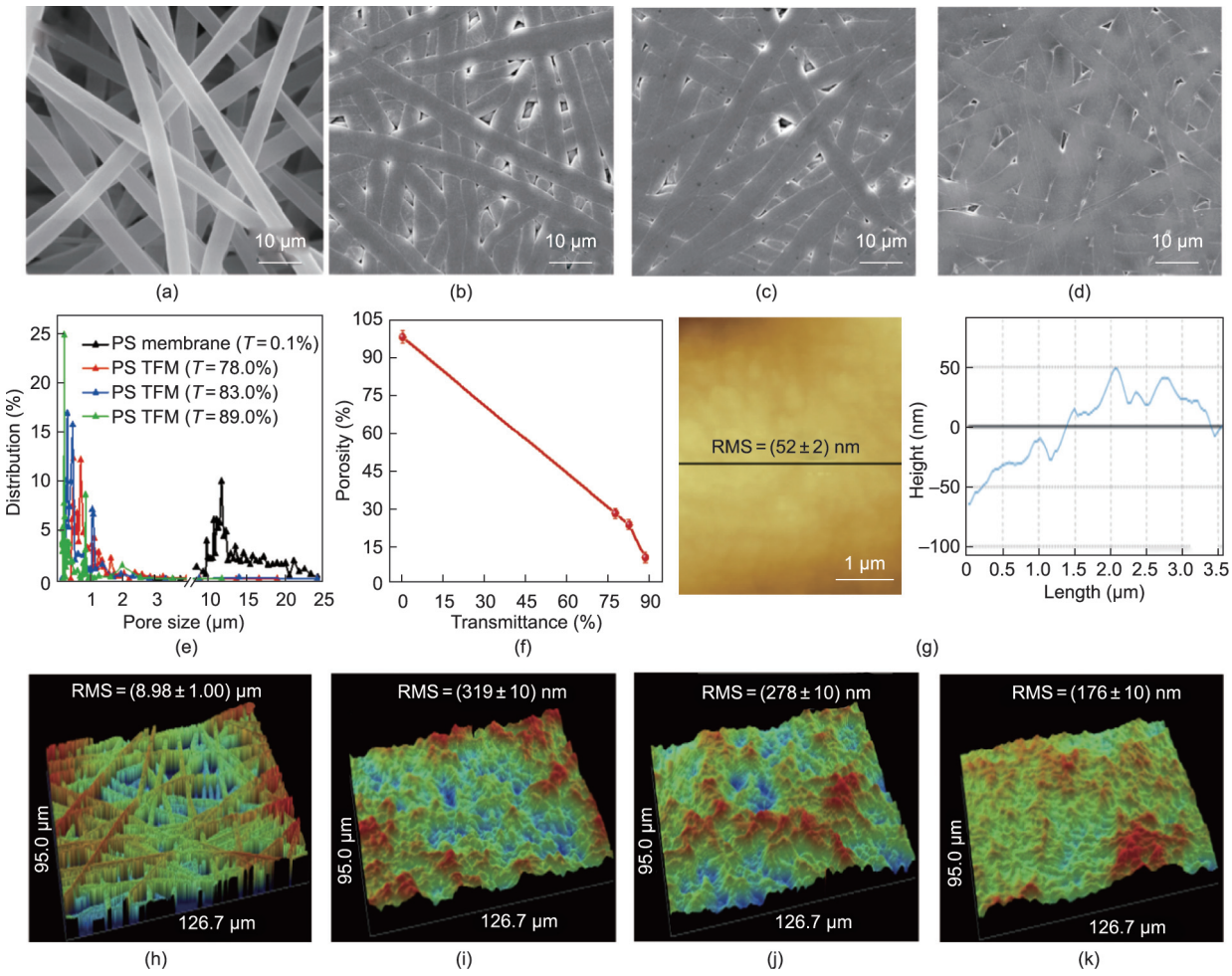

Fig. 2. Morphologies and pore structures. SEM images of PS fibrous membranes with different transmittance values of (a) 0.1%, (b) 78.0%, (c) 83.0%, and (d) 89.0%. (e) Pore size distributions and porosities of (a)–(d) (*T*: transmittance). (f) Relationship between transmittance and porosity. (g) AFM line scan of TFM with RMS of (52 ± 2) nm. (h)–(k) Optical profilometry images of PS fibrous membranes in (a)–(d).

and the fibers caused the reflection loss of light at the interface between the two components. According to Fresnel's law [46], $m = \left(\frac{n-1}{n+1}\right)^2$, where m stands for reflection loss and n refers to the relative refractive index of two different media, where the refractive index of air is 1; the reflection loss increased with an increase in the difference in the refractive indices. It was determined that a high amount of light was reflected onto the surface of the fibrous membrane and that light was scattered inside the fibrous membrane. ③ Membrane thickness. The thicker the fibrous membrane, the greater the decrease in light intensity, and the more difficult it is for light to pass through. Therefore, it is difficult to achieve transparency of fibrous membranes for these reasons.

Considering these factors, a simple and effective strategy using electrospinning followed by mechanical pressing was realized to fabricate TFMs. Pure PS without impurities was used to prepare the fibrous membrane via electrospinning, and the obtained fibrous membrane had a smooth surface and few internal defects. After pressing, the fluffy fibrous membrane became dense, and the surface roughness of the membrane decreased from micrometers to nanometers, resulting in a reduction in the reflection loss and a dramatic reduction in thickness. Meanwhile, a large amount of air was expelled, which significantly reduced the reflection loss at the interface between the fibers and air. Hence, the light transmittance of the fibrous membrane was greatly improved and the fibrous membrane became transparent.

Surprisingly, the PS TFM exhibited an interesting haze phenomenon. A pattern with grid lines was designed to show the image effects of the PS TFM (Figs. 3(b) and (c)). When the membrane contacted the pattern, all grid lines were clearly visible. However, both the parallel and vertical lines were diminished when the membrane was placed 10 mm above the grid lines. As displayed in Fig. 3(d), the left and right photographs show how the light arrived on the blackboard without a TFM and with the PS TFM, respectively. When light passed through the PS TFM, the intensity of the light diffused. Such high haze was attributed to the membrane still having numerous interfaces between the fibers and air, which led to small-angle scattering inside the membrane. In addition to its unique optical properties, the PS TFM also exhibited excellent mechanical properties (Fig. 3(e)), including high tensile fracture strength (~148 MPa), nearly 78 times that of a pristine fluffy PS membrane (~1.9 MPa). However, the strain tolerance of the PS TFM was sharply reduced owing to the close contact and the significant increase in interaction points among the fibers after pressing. This allowed the membrane to bear a higher external force and reduce slipping among the fibers. Therefore, the fracture strength significantly increased and elongation of the PS TFM decreased. Moreover, the TFMs fabricated via the two-step

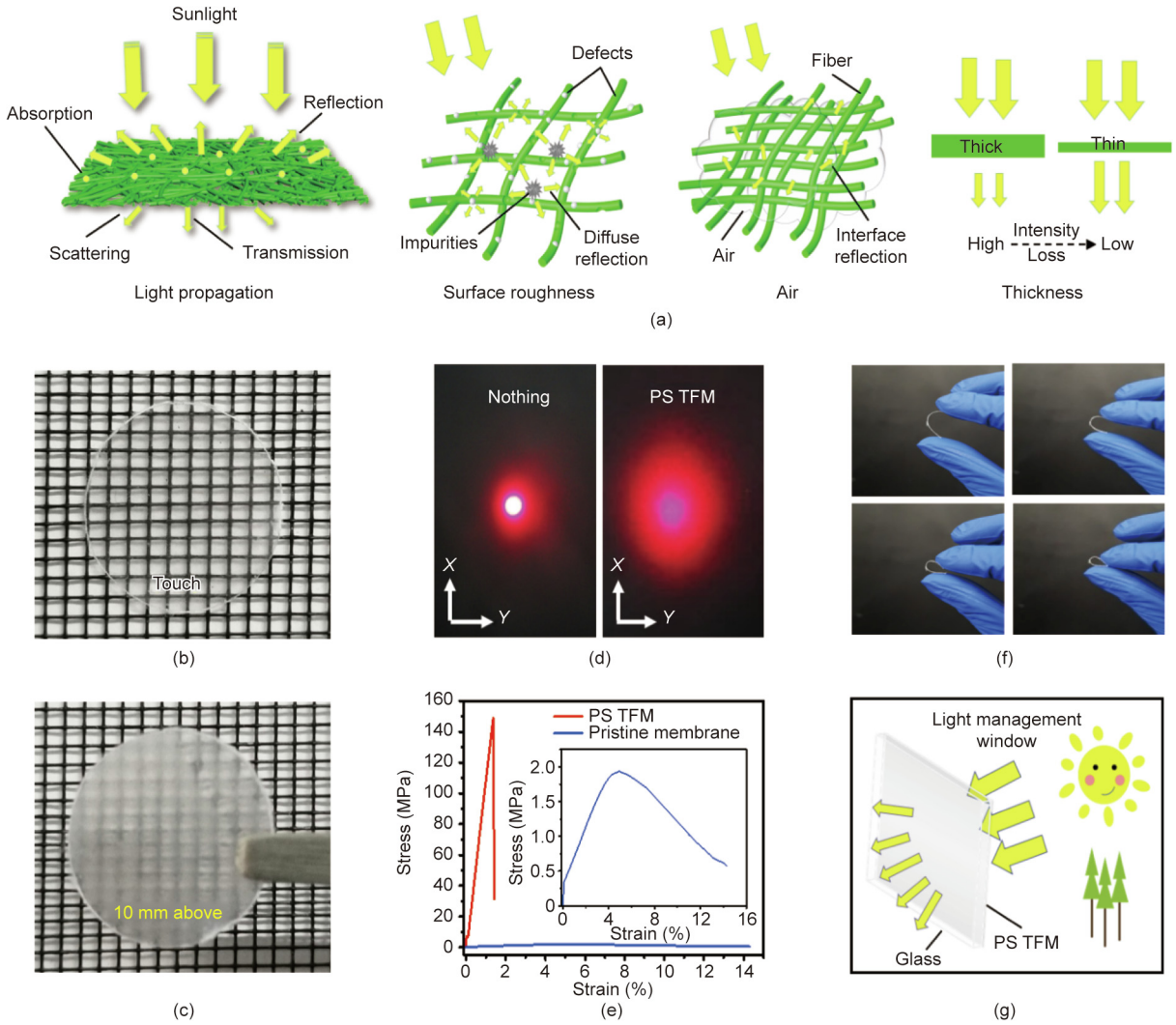

Fig. 3. Mechanism for determining the optical and mechanical properties of PS TFMs. (a) Schematic of the mechanism of light propagation for fibrous membranes. TFMs placed (b) directly onto the grids and (c) 10 mm above the grids. (d) Images of the scattered light spot: Left is without TFM, and right is with PS TFM. (e) Tensile stress–strain curves of PS TFM and pristine PS membrane (inset: the curve of pristine PS membrane at large magnification). (f) Optical images of TFMs showing outstanding mechanical properties and flexibility. (g) Schematic showing the light management of a glass window using PS TFMs.

approach were flexible, which was attributed to the continuous polymer fibrous networks, as shown in Fig. 3(f). Such a duality in mechanical properties may lead to applications in certain fields. For example, as shown in Fig. 3(g), the PS TFM could be used for light management when combined with glass windows for future applications. The membrane prevented strong light from directly shining into a room, hence the indoor light was dimmer, with open curtains and lights off.

Flexible transparent conductive films have become increasingly popular with the rapid development of flexible electronic devices in recent years. They include materials such as carbon nanotubes [47,48], graphene [49], and metallic networks [40,50,51], which are usually supported by substrates such as PET or glass and require complex manufacturing processes. Flexible, transparent, fiber-based conductive membranes were prepared using the electrospun PS TFMs and included the addition of AgNWs during vacuum-assisted filtration. AgNWs exhibit a very low resistivity of 1.6×10^{-8} Ω·m and are widely used as conductive media.

A schematic of the fabrication of the TFM/AgNW nanocomposite conductive membranes is presented in Fig. 4(a). The fibrous membrane was cut into circular shapes with diameters of 20 mm, followed by hot-pressing. The purpose of the hot-pressing treatment was to densify and flatten the surface of the fibrous membrane and reduce the surface fluidity to prepare it for AgNW loading. Fig. 4(b) shows an optical image of the hot-pressed membrane; compared with the pristine fluffy fibrous membrane (Fig. 1(b)), the fluffiness was eliminated (Appendix A Fig. S9) and the thickness was reduced. Then, the AgNWs were loaded onto the surface of the fibrous membrane via vacuum-assisted filtration. As seen in the SEM image of the hot-pressed membrane with AgNWs (Fig. 4(c)), the surface morphology of the fibrous membrane changed from loose and uneven (Fig. 2(a)) to dense and smooth, which reduced the leakage of AgNWs. The AgNWs formed a uniform network structure because the framework of the fibrous membrane decreased aggregation of the AgNWs. This caused the composite to exhibit high conductivity. In contrast, very few AgNWs were present on the untreated PS fibrous membrane (Appendix A Fig. S10). After drying, the circular-shaped membrane containing AgNWs was pressed under high pressure to form a transparent, fiber-based, conductive membrane. An optical image of the TFM/AgNW conductive membrane is shown in Fig. 4(d). Figs. 4(e)–(i) show the SEM images of TFM/AgNW nanocomposite conductive membranes containing different AgNW masses of 0.4, 0.6, 0.8, 1.0, and 1.2 mg, respectively. The

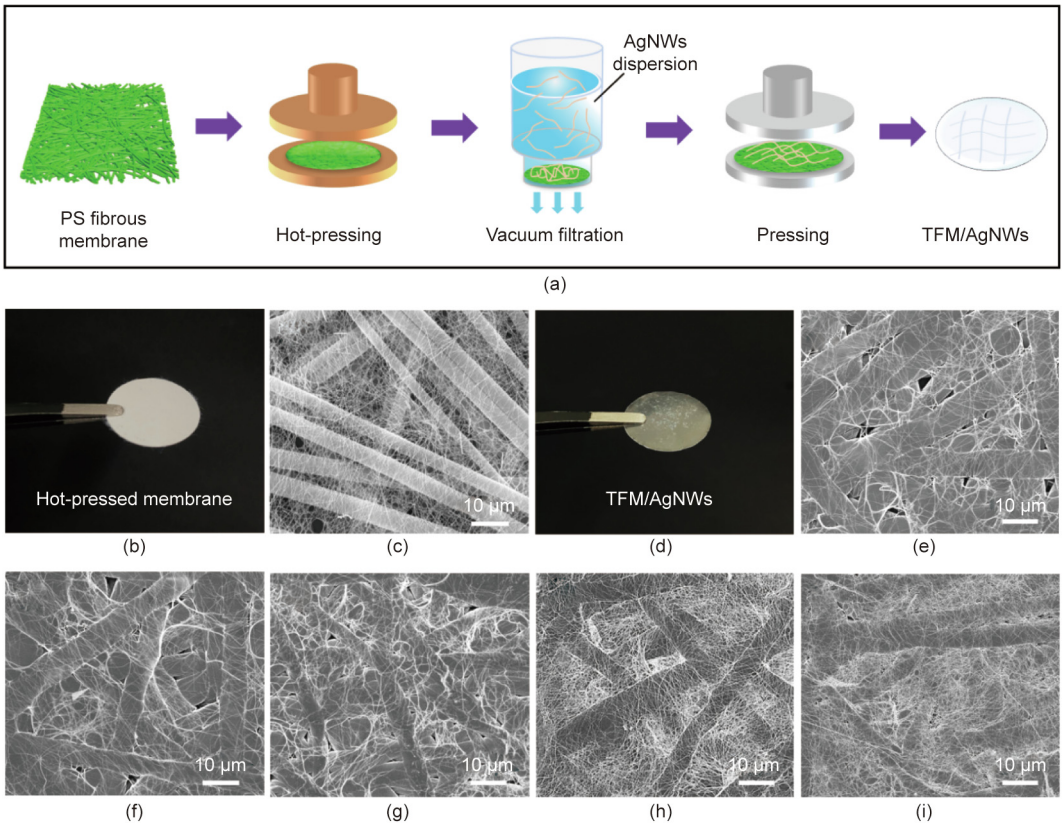

Fig. 4. Fabrication and micromorphology of the TFM/AgNWs. (a) Schematic illustrating the fabrication of TFM/AgNW nanocomposite conductive membranes. (b) Optical image of a hot-pressed membrane (d = 20 mm). (c) SEM image of a hot-pressed membrane covered with AgNWs. (d) Optical image of TFM/AgNWs (d = 20 mm). SEM images of the TFM/AgNW nanocomposite conductive membranes with different AgNW masses of (e) 0.4, (f) 0.6, (g) 0.8, (h) 1.0, and (i) 1.2 mg.

TFM/AgNW nanocomposite conductive membranes displayed an even distribution of AgNWs. With an increase in the mass of AgNWs, more highly efficient conductive networks were obtained because more junction points were generated.

Fig. 5(a) demonstrates the XRD patterns of the pure PS TFM and the conductive TFM/AgNW membrane with the increasing content of AgNWs. The conductive nanocomposite membranes presented similar diffraction peaks at 2θ = 38.12° and 44.28°, while no distinct diffraction peak was apparent for the pure PS TFM. Diffraction peaks at 2θ = 9.94° and 19.28° belonged to PS. The silver crystal planes of (111) and (200) indicated the face-centered cubic (fcc) crystalline silver. Furthermore, the intensity of the diffraction peaks at 2θ = 38.12° and 44.28° increased gradually as the AgNW content increased. Fig. 5(b) shows the transmittance of pure PS TFM and conductive TFM/AgNW nanocomposite membranes with different amounts of AgNWs in the visible light region (400–800 nm). The pure PS TFM and the conductive nanocomposite membranes with low AgNW content had high transparency, particularly pure PS TFM with the transmittance of 89.0% at 550 nm. The resistance and transmittance of the conductive membranes with different AgNW contents are shown in Fig. 5(c) and Fig. S11 in Appendix A. The transmittances (at 550 nm) of the nanocomposite conductive membranes covered with 0.4, 0.6, 0.8, 1.0, and 1.2 mg of AgNWs were 82.0%, 80.0%, 78.0%, 72.0%, and 64.0%, respectively. With the increasing AgNW mass, the optical transmittance gradually decreased because of more scattering and reflection of light. The conductive membranes exhibited a sheet resistance of approximately 50 $\Omega{\cdot}sq^{-1}$ at a low AgNW mass (0.4 mg) because of the sparsely distributed AgNWs and very few junction points. As the mass of AgNWs increased to 1.0 mg, the sheet resistance rapidly decreased to 3.5 $\Omega{\cdot}sq^{-1}$, which was much less than that of ITO (> 50 $\Omega{\cdot}sq^{-1}$) and graphene synthesized via chemical vapor deposition (> 250 $\Omega{\cdot}sq^{-1}$), due to the formation of numerous junction points and efficiently conductive AgNW networks. With the higher AgNW mass of 1.2 mg, there was a very small resistance drop to 3.0 $\Omega{\cdot}sq^{-1}$ because of an increase in the junction resistance between the AgNWs. The relationship between sheet resistance and transmittance can be utilized in fabricating transparent conductive membranes with the required sheet resistance to satisfy the demands of different applications.

The conductive TFM/AgNW nanocomposite membranes were flexible and bendable. A bending test was performed to examine the mechanical durability of the TFM/AgNW membranes, and the results were compared with those of ITO/PET conductive films (150 $\Omega{\cdot}sq^{-1}$), as shown in Figs. 5(d) and (e). The TFM/AgNW membranes were bent from flat to the radius of 3 mm (Fig. 5(d)), or repeatedly bent to 4 mm over 800 cycles (Fig. 5(e)). Upon examination of the TFM/AgNW membrane after both bending methods, no significant change in the electrical conductivity was observed. In contrast, the ITO/PET film exhibited severe degradation in conductivity after bending to 4 mm or bending to 4 mm for more than 150 cycles. Fig. 5(e) shows that the TFM/AgNW membranes preserved their mechanical robustness and conductivity through many cycles of dynamic bending tests. Fig. 5(f) shows the stability of the membranes during continuous charging. After 7200 s, the resistance of the conductive membranes only increased by 0.08 $\Omega{\cdot}sq^{-1}$, confirming the stable conductivity. An organic light emitting diode (OLED) lamp was illuminated via the TFM/AgNW transparent conductive membrane attached to a leaf, as shown in Fig. 5(g), proving that the membrane had a high conductivity. Optical images of the

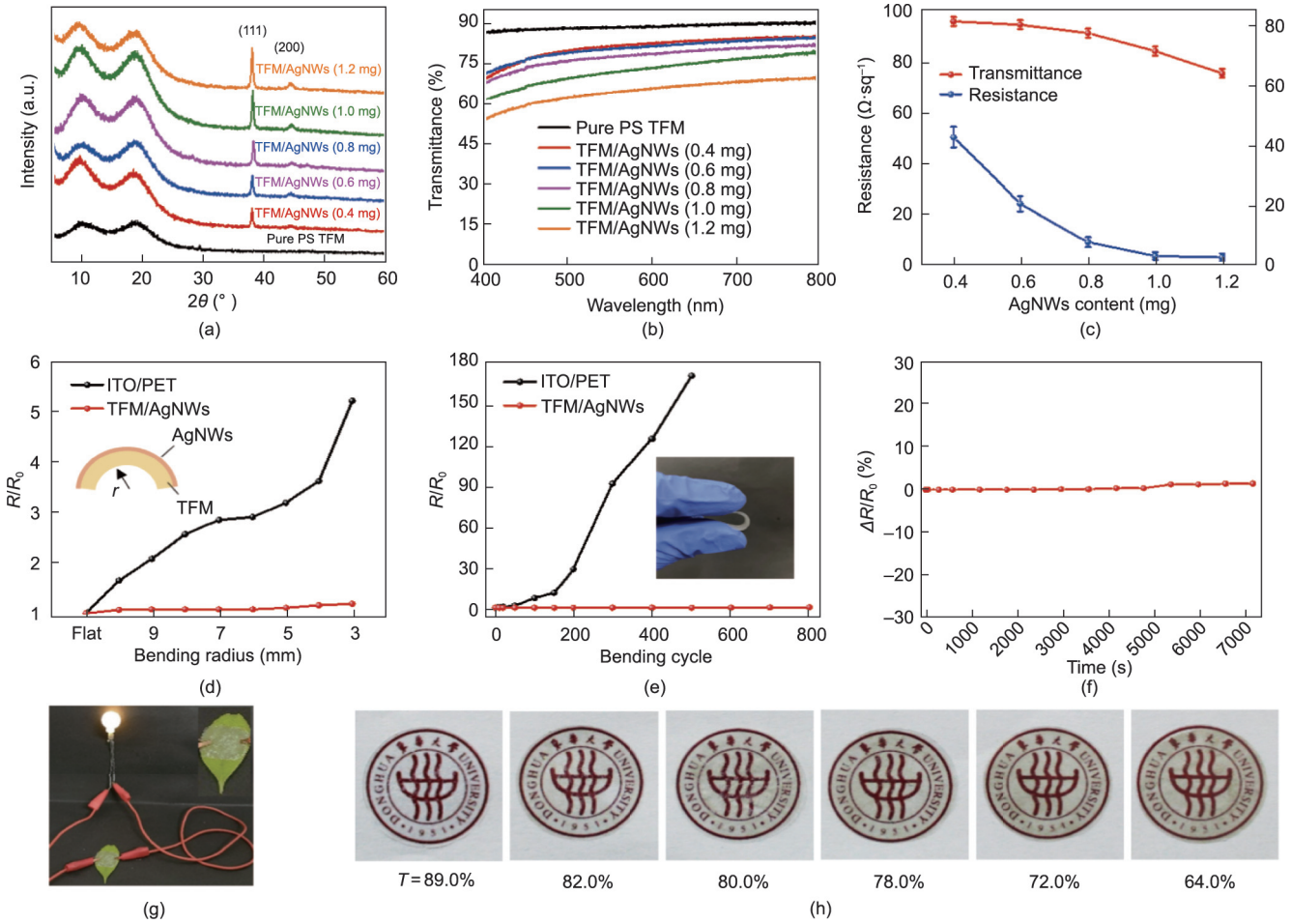

Fig. 5. Optical and electrical properties of TFM/AgNWs. (a) XRD patterns and (b) transmittance of the pure PS TFM and the conductive TFM/AgNW nanocomposite membranes with increasing content of AgNWs. (c) Resistance and transmittance of conductive membranes with different AgNW contents. (d) Sheet resistance versus bending radius for bendable transparent conductive membranes comprising ITO/PET and TFM/AgNWs (inset: the direction of bending; R_0 and R represent sheet resistance before and after bending tests respectively; and r represents the bending radius). (e) Variations in the resistance of ITO/PET and TFM/AgNWs, which were both bent to the radius of 4 mm; inset: bending display. (f) Stability testing of a TFM/AgNW conductive membrane during continuous charging. (g) Photo of transparent conductive membrane used to illuminate an OLED lamp (inset: transparent membrane (78.0%, 9 $\Omega \cdot sq^{-1}$) attached to a leaf). (h) Optical photographs of the transparent conductive membranes (containing 0–1.2 mg of AgNWs) with different transmittances (at 550 nm) of 89.0%, 82.0%, 80.0%, 78.0%, 72.0%, and 64.0%. The background is the logo of Donghua University, Shanghai, China. a.u.: arbitrary units; 2θ: scattering angle.

transparent conductive membranes with different AgNW masses are presented in Fig. 5(h). The transmittance decreased from 89.0% to 64.0% with the increase in the mass of AgNWs, and the background used was the logo of Donghua University, Shanghai, China.

4. Conclusions

In conclusion, we demonstrated the fabrication of transparent and porous electrospun fibrous membranes via a facile but effective method and summarized the relationship between the transparency performance and molecular structure of polymers for the first time. The fibrous morphology and porosity of the membranes were preserved after a mechanical pressing process, and the effects of porosity and surface roughness on the transmittance were investigated. In addition, the mechanism of the transparency of the fibrous membranes was systematically revealed. The TFMs exhibited excellent flexibility, high optical transmittance (~89% at 550 nm along with high haze), and high porosity and mechanical strength (~148 MPa). Such porous, transparent, and fibrous membranes will play key roles in the fields of intelligent wearables, electronic skin, air filtration, and tissue engineering. Moreover, the fabrication of transparent and flexible nanocomposite membranes based on highly transparent electrospun fibrous membranes was demonstrated. Composite membranes containing AgNWs also exhibited excellent electrical conductivities (to compete with ITO films) as well as notable mechanical performance (to bear abundant bending stresses) and can be widely used in flexible optoelectronic devices.

Acknowledgments

This work is supported by the National Natural Science Foundation of China (52073052 and 51925302), the Program for Professor of Special Appointment at Shanghai Institutions of Higher Learning (TP2016019), the Fundamental Research Funds for the Central Universities, and Graduate Student Innovation Fund of Donghua University (CUSF-DH-D-2020009).

Compliance with ethics guidelines

Chao Wang, Jing Zhao, Peng Zhang, Xianfeng Wang, Jianyong Yu, and Bin Ding declare that they have no conflict of interest or financial conflicts to disclose.

Appendix A. Supplementary data

Supplementary data to this article can be found online at https://doi.org/10.1016/j.eng.2021.02.018.

References

[1] Meng L, Bian R, Guo C, Xu B, Liu H, Jiang L. Aligning Ag nanowires by a facile bioinspired directional liquid transfer: toward anisotropic flexible conductive electrodes. Adv Mater 2018;30(25):1706938.
[2] Singh VK, Ravi SK, Sun W, Tan SC. Transparent nanofibrous mesh self-assembled from molecular LEGOs for high efficiency air filtration with new functionalities. Small 2017;13(6):1601924.
[3] Wang Y, Cheng J, Xing Y, Shahid M, Nishijima H, Pan W. Stretchable platinum network-based transparent electrodes for highly sensitive wearable electronics. Small 2017;13(27):1604291.
[4] Kang S, Cho S, Shanker R, Lee H, Park J, Um DS, et al. Transparent and conductive nanomembranes with orthogonal silver nanowire arrays for skin-attachable loudspeakers and microphones. Sci Adv 2018;4(8):eaas8772.
[5] Hecht DS, Hu L, Irvin G. Emerging transparent electrodes based on thin films of carbon nanotubes, graphene, and metallic nanostructures. Adv Mater 2011;23(13):1482–513.
[6] An BW, Heo S, Ji S, Bien F, Park JU. Transparent and flexible fingerprint sensor array with multiplexed detection of tactile pressure and skin temperature. Nat Commun 2018;9(1):2458.
[7] Gong M, Wan P, Ma D, Zhong M, Liao M, Ye J, et al. Flexible breathable nanomesh electronic devices for on-demand therapy. Adv Funct Mater 2019;29(26):1902127.
[8] Kim MW, An S, Seok H, Yoon SS, Yarin AL. Electrostatic transparent air filter membranes composed of metallized microfibers for particulate removal. ACS Appl Mater Interfaces 2019;11(29):26323–32.
[9] Chen R, Zhang X, Wang P, Xie K, Jian J, Zhang Y, et al. Transparent thermoplastic polyurethane air filters for efficient electrostatic capture of particulate matter pollutants. Nanotechnology 2019;30(1):015703.
[10] De Sio L, Ding B, Focsan M, Kogermann K, Pascoal-Faria P, Petronela F, et al. Personalized reusable face masks with smart nano-assisted destruction of pathogens for COVID-19: a visionary road. Chemistry 2021;27(20):6112–30.
[11] Yao Y, Tao J, Zou J, Zhang B, Li T, Dai J, et al. Light management in plastic–paper hybrid substrate towards high-performance optoelectronics. Energy Environ Sci 2016;9(7):2278–85.
[12] Wang Y, Yuan L, Tian H, Zhang L, Lu A. Strong, transparent cellulose film as gas barrier constructed via water evaporation induced dense packing. J Membr Sci 2019;585:99–108.
[13] Ye D, Lei X, Li T, Cheng Q, Chang C, Hu L, et al. Ultrahigh tough, super clear, and highly anisotropic nanofiber-structured regenerated cellulose films. ACS Nano 2019;13(4):4843–53.
[14] Niu X, Liu Y, Fang G, Huang C, Rojas OJ, Pan H. Highly transparent, strong, and flexible films with modified cellulose nanofiber bearing UV shielding property. Biomacromolecules 2018;19(12):4565–75.
[15] Huang J, Zhu H, Chen Y, Preston C, Rohrbach K, Cumings J, et al. Highly transparent and flexible nanopaper transistors. ACS Nano 2013;7(3):2106–13.
[16] Jin J, Lee D, Im HG, Han YC, Jeong EG, Rolandi M, et al. Chitin nanofiber transparent paper for flexible green electronics. Adv Mater 2016;28(26):5169–75.
[17] Huang J, Zhong Yi, Zhang L, Cai J. Extremely strong and transparent chitin films: a high-efficiency, energy-saving, and "Green" route using an aqueous KOH/Urea solution. Adv Funct Mater 2017;27(26):1701100.
[18] Zhu M, Song J, Li T, Gong A, Wang Y, Dai J, et al. Highly anisotropic, highly transparent wood composites. Adv Mater 2016;28(26):5181–7.
[19] Zhu M, Wang Y, Zhu S, Xu L, Jia C, Dai J, et al. Anisotropic, transparent films with aligned cellulose nanofibers. Adv Mater 2017;29(21):1606284.
[20] Jia C, Chen C, Mi R, Li T, Dai J, Yang Z, et al. Clear wood toward high-performance building materials. ACS Nano 2019;13(9):9993–10001.
[21] Song J, Chen C, Zhu S, Zhu M, Dai J, Ray U, et al. Processing bulk natural wood into a high-performance structural material. Nature 2018;554(7691):224–8.
[22] Li T, Zhu M, Yang Z, Song J, Dai J, Yao Y, et al. Wood composite as an energy efficient building material: guided sunlight transmittance and effective thermal insulation. Adv Energy Mater 2016;6(22):1601122.
[23] Zhou T, Wang JW, Huang M, An R, Tan H, Wei H, et al. Breathable nanowood biofilms as guiding layer for green on-skin electronics. Small 2019;15(31):1901079.
[24] Wang X, Huang Z, Miao D, Zhao J, Yu J, Ding B. Biomimetic fibrous murray membranes with ultrafast water transport and evaporation for smart moisture-wicking fabrics. ACS Nano 2019;13(2):1060–70.
[25] Zhao J, Zhu W, Wang X, Liu L, Yu J, Ding B. Environmentally benign modification of breathable nanofibrous membranes exhibiting superior waterproof and photocatalytic self-cleaning properties. Nanoscale Horiz. 2019;4(4):867–73.
[26] Ge J, Zong D, Jin Q, Yu J, Ding B. Biomimetic and superwettable nanofibrous skins for highly efficient separation of oil-in-water emulsions. Adv Funct Mater 2018;28(10):1705051.
[27] Lim BH, Nirmala R, Navamathavan R, Kim HY. Flexible and conducting carbon nanofibers obtained from electrospun polyacrylonitrile/phosphoric acid nanofibers. J Nanosci Nanotechnol 2016;16(1):1033–7.
[28] Chen LF, Lu Y, Yu L, Lou XW. Designed formation of hollow particle-based nitrogen-doped carbon nanofibers for high-performance supercapacitors. Energy Environ Sci 2017;10(8):1777–83.
[29] Si Y, Ren T, Li Y, Ding B, Yu J. Fabrication of magnetic polybenzoxazine-based carbon nanofibers with Fe_3O_4 inclusions with a hierarchical porous structure for water treatment. Carbon 2012;50(14):5176–85.
[30] Shan H, Wang X, Shi F, Yan J, Yu J, Ding B. Hierarchical porous structured SiO_2/SnO_2 nanofibrous membrane with superb flexibility for molecular filtration. ACS Appl Mater Interfaces 2017;9(22):18966–76.
[31] Shan H, Dong X, Cheng X, Si Y, Yu J, Ding B. Highly flexible, mesoporous structured, and metallic Cu-doped C/SiO_2 nanofibrous membranes for efficient catalytic oxidative elimination of antibiotic pollutants. Nanoscale 2019;11(31):14844–56.
[32] Si Y, Wang X, Dou L, Yu J, Ding B. Ultralight and fire-resistant ceramic nanofibrous aerogels with temperature-invariant superelasticity. Sci Adv 2018;4(4):eaas8925.
[33] Wang X, Ding B, Yu J, Wang M. Engineering biomimetic superhydrophobic surfaces of electrospun nanomaterials. Nano Today 2011;6(5):510–30.
[34] Wang X, Ding B, Sun G, Wang M, Yu J. Electro-spinning/netting: a strategy for the fabrication of three-dimensional polymer nano-fiber/nets. Prog Mater Sci 2013;58(8):1173–243.
[35] Li D, Xia Y. Electrospinning of nanofibers: reinventing the wheel? Adv Mater 2004;16(14):1151–70.
[36] Bergshoef MM, Vancso GJ. Transparent nanocomposites with ultrathin, electrospun nylon-4,6 fiber reinforcement. Adv Mater 1999;11(16):1362–5.
[37] Kim IC, Kim TH, Lee SH, Kim BS. Extremely foldable and highly transparent nanofiber-based electrodes for liquid crystal smart devices. Sci Rep 2018;8(1):11517.
[38] Zhao Y, Wang X, Zhang Q, Li Ni. Preparation of transparent polyacrylonitrile reinforced polyurethane film and application as temperature monitor. Polym Eng Sci 2018;58(11):1905–10.
[39] Liu L, Li HY, Fan YJ, Chen YH, Kuang SY, Li ZB, et al. Nanofiber-reinforced silver nanowires network as a robust, ultrathin, and conformable epidermal electrode for ambulatory monitoring of physiological signals. Small 2019;15(22):1900755.
[40] Zhang C, Cai J, Liang C, Khan A, Li WD. Scalable fabrication of metallic nanofiber network via templated electrodeposition for flexible electronics. Adv Funct Mater 2019;29(35):1903123.
[41] Zhang S, Liu H, Tang N, Ge J, Yu J, Ding B. Direct electronetting of high-performance membranes based on self-assembled 2D nanoarchitectured networks. Nat Commun 2019;10(1):1458.
[42] Liu H, Zhang S, Liu L, Yu J, Ding BZSC, Liu LF, et al. A fluffy dual-network structured nanofiber/net filter enables high-efficiency air filtration. Adv Funct Mater 2019;29(39):1904108.
[43] Zhang S, Liu H, Tang N, Ali N, Yu J, Ding B. Highly efficient, transparent, and multifunctional air filters using self-assembled 2D nanoarchitectured fibrous networks. ACS Nano 2019;13(11):13501–12.
[44] Khalid B, Bai X, Wei H, Huang Ya, Wu H, Cui Yi. Direct blow-spinning of nanofibers on a window screen for highly efficient $PM_{2.5}$ removal. Nano Lett 2017;17(2):1140–8.
[45] Zuo F, Zhang S, Liu H, Fong H, Yin X, Yu J, et al. Free-standing polyurethane nanofiber/nets air filters for effective PM capture. Small 2017;13(46):1702139.
[46] Monzon JJ, Sanchez-Soto LL. Algebraic structure of Fresnel reflection and transmission coefficients at an interface. Optik 1999;110(7):309–12.
[47] Zhang M, Fang S, Zakhidov AA, Lee SB, Aliev AE, Williams CD, et al. Strong, transparent, multifunctional, carbon nanotube sheets. Science 2005;309(5738):1215–90.
[48] Havel M, Behler K, Korneva G, Gogotsi Y. Transparent thin films of multiwalled carbon nanotubes self-assembled on polyamide 11 nanofibers. Adv Funct Mater 2008;18(16):2322–7.
[49] Fuh YK, Kuo CC, Huang ZM, Li SC, Liu ER. A transparent and flexible graphene-piezoelectric fiber generator. Small 2016;12(14):1875–81.
[50] Lin S, Bai X, Wang H, Wang H, Song J, Huang K, et al. Roll-to-roll production of transparent silver-nanofiber-network electrodes for flexible electrochromic smart windows. Adv Mater 2017;29(41):1703238.
[51] Wu H, Kong D, Ruan Z, Hsu PC, Wang S, Yu Z, et al. A transparent electrode based on a metal nanotrough network. Nat Nanotechnol 2013;8(6):421–5.